NRL Report 6942

The Effect of Surface Finishing on Structural-Ceramic Failure

K. R. McKinney

Ocean Materials Criteria Branch
Ocean Technology Division

and

C. M. Herbert

Research Devices Facility
Electronics Division

November 5, 1969

NAVAL RESEARCH LABORATORY
Washington, D.C.

This document has been approved for public release and sale; its distribution is unlimited.

CONTENTS

Abstract	ii
Problem Status	ii
Authorization	ii
INTRODUCTION	1
PREPARATION OF TEST SPECIMENS	1
Final Finishing Grits	1
Surface Paralleling	1
Surface Final Finish	3
EXPERIMENTAL PROCEDURE	3
COMPUTATION	3
DISCUSSION OF RESULTS	6
CONCLUSIONS	6
ACKNOWLEDGMENT	7
REFERENCES	8
APPENDIX A - Determination of Bearing Radius	9
APPENDIX B - Surface Analysis	20

ABSTRACT

A relationship between fracture strength and surface finish of brittle nonmetallic materials was examined and related to surface crack theory. An experimental illustration used AlSiMag 614, a 94% pure alumina with a near zero porosity. Specimen disks 3.625 + 0.031 in. in diameter by 0.085 + 0.010 in. thick were prepared, each having a specific surface finish. Testing was done with a biaxial ball and ring test. Observations were made regarding other materials and other abrasive powders.

PROBLEM STATUS

This is an interim report on one phase of a continuing problem.

AUTHORIZATION

NRL Problem F01-05
Project A-32-520/652/69 R0070201

Manuscript submitted May 27, 1969.

THE EFFECT OF SURFACE FINISHING ON STRUCTURAL-CERAMIC FAILURE

INTRODUCTION

Because of ceramics' high compressive strength, chemical inertness, and mechanical integrity over a wide range of temperatures, there is a great interest in their use as structural materials. Any such use makes it necessary at times to change the shape of the piece of ceramic through machining. This "is a rather brutal treatment" (1) and may impair the strength of brittle materials such as ceramics. Even if components could always be used "as fired" this would not guarantee the absence of flaws that could be equally dangerous. It seemed profitable, therefore, to investigate how the surface-crack fracture theory reported by Tiffany and Lorenz (2) could be applied to scratches induced by grinding procedures.

PREPARATION OF TEST SPECIMENS

The specimens were chosen from AlSiMag 614 material, on hand, for which as-fired fracture data was already available. These specimens, received from the American Lava Corporation as disks 3.625 ± 0.031 in. in diameter by 0.100 ± 0.005 in. thick, were in a rough form far from being flat and parallel, making them ideal for this study.

Specimens were prepared for testing as follows: first, five grits for final finish were chosen; second, the surfaces of the specimens were ground parallel in a machine shop; and third, the final finish was applied to one surface.

Final Finishing Grits

The five final-finish SiC grits were chosen on the basis of availability of abrasive, information about the abrasive, and its capability of successfully finishing the chosen specimens. All grits were acquired from the Carborundum Company. A listing of grit numbers and their sizes is shown in Table 1 (3,4).

Surface Paralleling

An attempt was made to make the disks flat and parallel by grinding them on a cast iron lap using a free abrasive of 100-grit silicon carbide and water, but AlSiMag 614 is of a hardness that proved this method to be too slow. The process was repeated using a free abrasive of 240-grit boron carbide and water. Both of these methods removed material but, because the AlSiMag samples were so far out of flatness, it was decided in the interest of time and money to surface grind the disks. By the use of a vacuum chuck, each sample was ground singly on a Gallmeyer and Livingston surface grinder as shown in Fig. 1. A first attempt was made with a 46-grit silicon-carbide grinding wheel of 12-in. diameter and 3/4-in. wide cooled by commercially available Cimcool. The grinding wheel was accurately balanced and trued prior to starting. The hardness of the AlSiMag caused the grinding wheel to "burn," and the decision was made to go to a diamond grinding wheel. The diamond wheel, 8-in. diameter, 1/2-in. wide resinoid bond, 100 grit, and 100 concentration, was also accurately balanced and trued, and again the coolant used was

Table 1
Breaking Stress For Various Surface Finishes of AlSiMag 614
As Compared to Those Computed Using Surface-Crack Fracture Theory

Finish	Grit Size (microns)	Number of Specimens	Average σ_{EXP}	σ_{SC}	Two average standard deviations below average σ_{EXP}
			($10^3 \times$ lbs/in.^{2})		
As Paralled	–	4	41.5	–	33.8
As Fired	–	25	36.5	–	30.0
SiC 600 grit	17 (4)	6	36.5	48.5	30.0
SiC 400 grit	26 (3)	5	35.4	42.5	29.4
SiC 220 grit	62 (3)	5	31.3	27.5	26.6
SiC 100 grit	149 (3)	5	25.2	18.0	21.6
SiC 70 grit	210 (3)	5	21.9	15.0	19.1

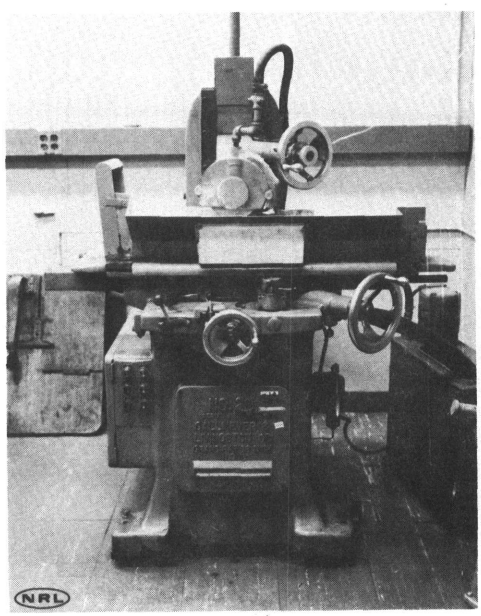

Fig. 1 - The Gallmeyer and Livingston surface grinder used to parallel the surfaces of the AlSiMag 614 ceramic specimens

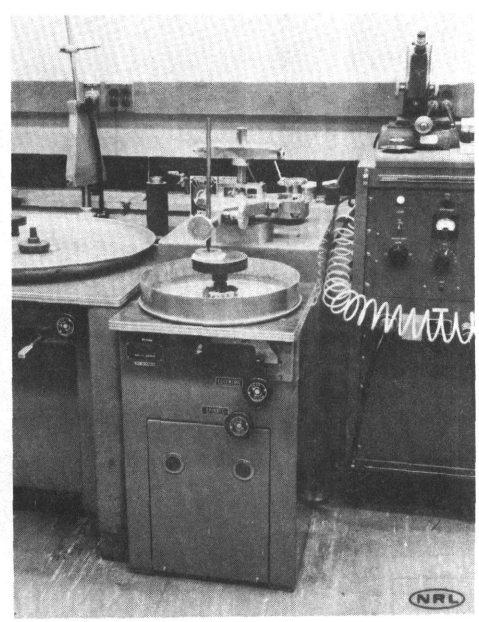

Fig. 2 - The Strasbaugh optical grinding machine used to final-finish the AlSiMag 614 ceramic specimens

Cimcool. The disks were precisely ground flat by advancing the down feed 0.001 in. per cut while roughing and 0.0002 in. per cut when finishing. The disks were turned over and again held by the vacuum chuck to grind the opposite side accurately parallel. The disks were now ready to be ground with the proper chosen grit of silicon carbide abrasive.

Surface Final Finish

A stainless steel blocking body was waxed to one face of each AlSiMag disk with Universal Shellac Company's No. 48 blocking wax. One face of the disk was then ground using a 6-in.-diameter plane cast iron lap on a Strasbaugh optical grinding machine; Fig. 2, the lap rotated at 20-25 rpm and the disk automatically oscillated across the turning lap. The free abrasive was fed to the lap in a slurry of water, and the lapping procedure was continued until the entire surface of the AlSiMag 614 disk was uniformly ground. A close-up view of this procedure is shown in Fig. 3.

The stainless steel blocking body was then warmed on a hot plate and the AlSiMag disk slid off. When cool the disk was ultrasonically cleaned in a solution of trichloroethylene and acetone.

Fig. 3 - A detailed view of AlSiMag 614 being ground on the Strasbaugh optical grinding machine

EXPERIMENTAL PROCEDURE

All tests were made using an electrohydraulic, closed loop controlled, testing machine (5), Fig. 4. Specimen fracture was induced using a biaxial ring type test assembly, as seen in Fig. 5. Room atmospheric conditions were 75 ± 3°F and 50 ± 3% R.H. The testing was done as follows: one, place finished side of specimen down on the ring and visually center it; two, apply preprogrammed load, approximately 50 lb/min, until failure occurs, and three, record all information necessary for the reduction of data on the chart where the load data is recorded.

COMPUTATION

Since surface finishing is a process of placing many small scratches in a surface, it was decided that surface-crack fracture theory would be helpful in determining the finish

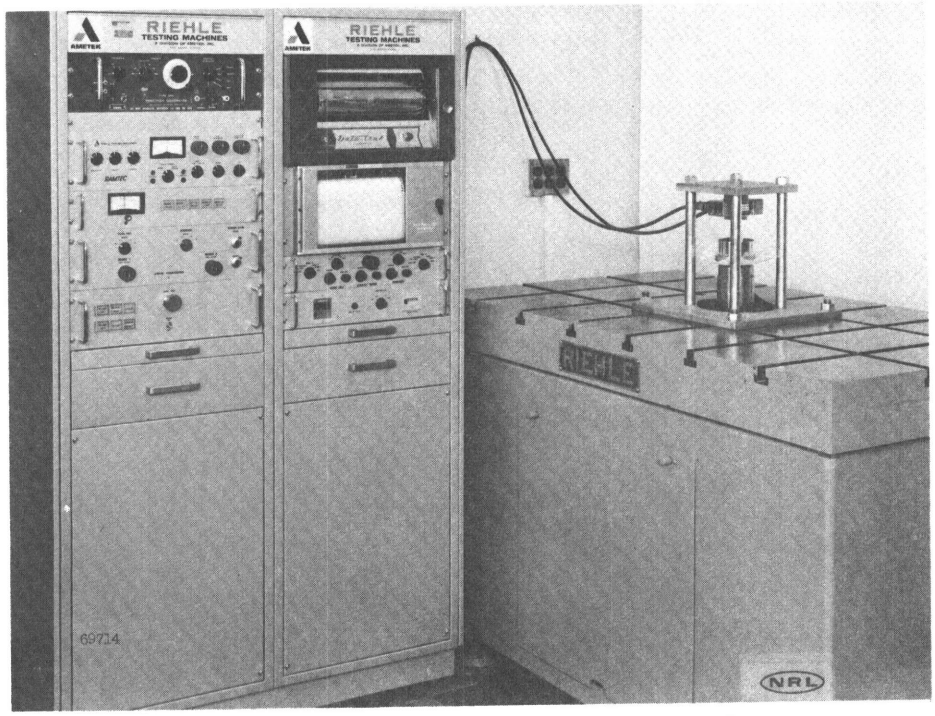

Fig. 4 - The test assembly and controls

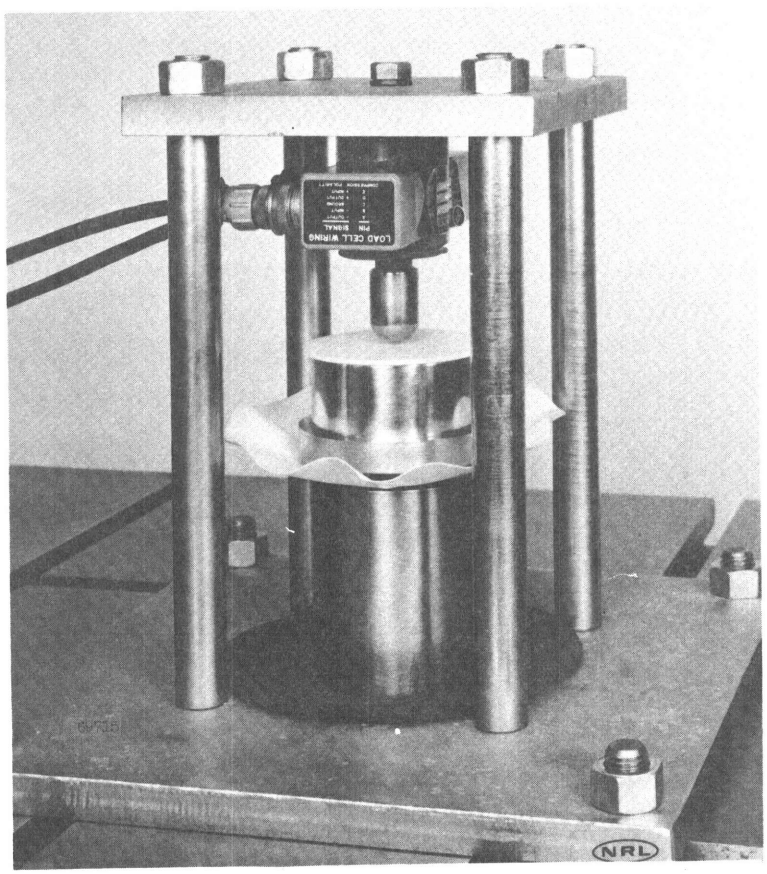

Fig. 5 - The test assembly as used in a test

necessary to obtain a given minimum strength for a ceramic material. Tiffany and Lorenz (2) show a graph, Fig. 6, simplifying the use of a surface crack equation based on the work of Irwin (6). The basic equation employed is

$$K_{Ic} = 1.1\sqrt{\pi}\,\sigma_{SC}\,(a/Q)^{1/2}, \tag{1}$$

where a = half crack scratch depth. Since the crack could be essentially a continuous scratch, the half crack length, C, is considered to be infinite. Therefore a/2C is 0. Also σ/σ_{ys} should have an upper limit of 1 for brittle ceramics. This value would give a Q of about 0.78. Substituting in this value and solving for σ_{SC} Eq. (1) becomes

$$\sigma_{SC} = \frac{K_{Ic}}{1.1\sqrt{\pi\, a/0.78}} \tag{2}$$

Since AlSiMag 614 probably has fracture properties about the same as other high-density, high-purity aluminas (7), a K_{Ic} of approximately 3×10^3 lb/in.$^{3/2}$ is assumed. Also, the deepest possible scratch is assumed to be the diameter of the grit. Stress predictions for each finish are listed in Table 1.

The experimentally determined fracture stress is found by (8) the equation

$$\sigma_{EXP} = s_r = \frac{3W}{2\pi mt^2}\left[m + (m+1)\log\frac{\alpha}{r_o} - (m-1)\frac{r_o^2}{4\alpha^2}\right], \tag{3}$$

where s_r = radial stress, W = load, m = 1/Poisson's ratio, t = thickness of specimen, α = radius of specimen under test, and r_o = radius of bearing area. For reasons to be explained later, Eq. (7) of Appendix A was used in place of Eq. (3). Each of these stresses are shown for comparison in Table 1.

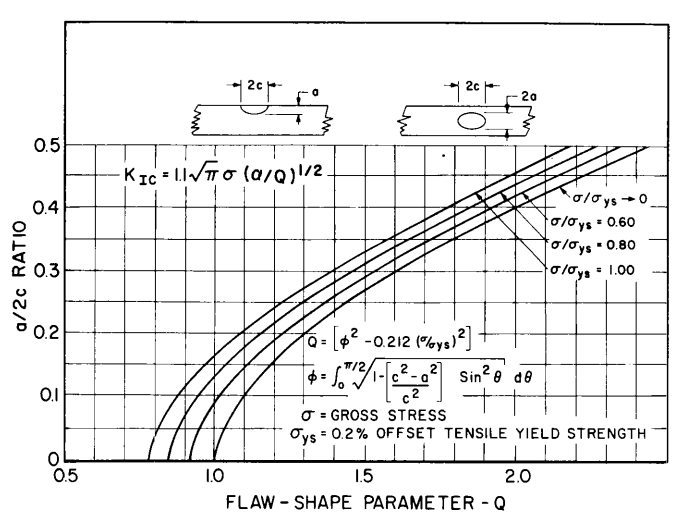

Fig. 6 - Figure from Tiffany and Lorenz (2) used to simplify the use of surface-crack fracture equations derived by Irwin (4)

DISCUSSION OF RESULTS

Results shown in Table 1 would seem to indicate a relationship between σ_{EXP} and σ_{SC}. Figure 7 shows plots of σ_{EXP} and σ_{SC} vs grit size (SiC) in microns of finishing abrasive. The upper bound of σ_{EXP} in the figure is representative of the average maximum fracture strength for the various grit sizes. The problem with basing our discussion on these values is that they are obtained by giving equal weight to all values, high as well as low. Like a chain, the high values are not going to be of aid in a service application if low valued links are also present. Therefore the discussion will dwell around the lower bound of σ_{EXP} which represents the maximum fracture strength at an average two standard deviations below the upper bound. Since this would take in about 97% of all specimens, hence 97% of all surface, it would be more representative of the behavior of the material in a service application. Also, it does not seem too optimistic to hope that in the case of the remaining 3% it would not be much lower in quality, or that it be so degraded it could be reasonably inspected out. The representation of σ_{SC} is obtained by using Eq. (2), which, by inspection, can be seen to be invalid when approaching a zero scratch depth, for it predicts a σ_{SC} approaching ∞ for a scratch depth approaching zero. It is shown by data obtained at NRL (9), for a similar material, that the best of efforts to eliminate surface flaws does not quite double the fracture strength as compared to "as paralleled." Therefore it could not be expected that σ_{EXP} would approach σ_{SC} for small grit sizes. As we consider larger grit sizes we see that a crossover occurs and σ_{SC} becomes smaller than σ_{EXP}. It seems reasonable that there is a limit to the validity of the assumption about the relationship between the depth of scratch and the grit size. As the grit size becomes larger, the portion of the abrasive particles that penetrate the surface would decrease because of a larger diameter particle that must be embedded into the surface, and also because of a blunter scratch produced, Appendix B. This would mean that a of Eq. (2) would be assumed too large. The result would be that σ_{SC} would appear to be smaller than σ_{EXP}. This may mean that, once the crossover point of approximately 70 microns is reached, σ_{SC} might nearly duplicate σ_{EXP} for softer ceramics. An even greater separation would be expected for harder brittle materials.

By the use of Fig. 8, σ_{EXP}/σ_{SC} vs grit size, it is possible to determine the fracture stress for any brittle material having low porosity and surface hardness near the same as AlSiMag 614, provided the stress intensity factor, K_{Ic}, of the material and the SiC surface finish details are known. Figure 8 should be of some limited use for considering other brittle materials and polishing grits. For softer materials and/or harder grits, no change would be expected in Fig. 8 from 70 microns down to about 5 microns, since 100% depth of scratch was already assumed and well may be true. Below 5 microns grit size, Eq. (2) predicts strengths much larger than measured strength, because σ_{SC} approaches infinity. It is known that glazed materials should have strengths (9) of around twice those that would be obtained by simple extrapolation to zero grit size in Fig. 7; however, σ_{EXP} was not explored for grit sizes approaching zero. At above 70 microns, if the material is softer or the grit harder, σ_{EXP}/σ_{SC} should probably remain closer to 1. Care should be exercised in these cases since for them the use of Fig. 8 would result in an overestimation of the breaking stress. If the material is harder, or the grit softer, the curve in Fig. 8 should probably rise faster, since a smaller depth of scratch would result. The use of Fig. 8 would cause an underestimate, and thus a safety factor, provided the grit is capable of polishing the material.

CONCLUSIONS

1. A relationship between fracture stress and surface finish exists for low porosity ceramics.

2. By use of the relationship between experimental fracture stress and surface crack theory a prediction of fracture strength of ceramic materials with particular surface finishes can be made.

ACKNOWLEDGMENT

The authors are indebted to Mr. H. O. Ewing of NRL for sharing his experience on technical apparatus, resulting in the saving of numerous hours of work.

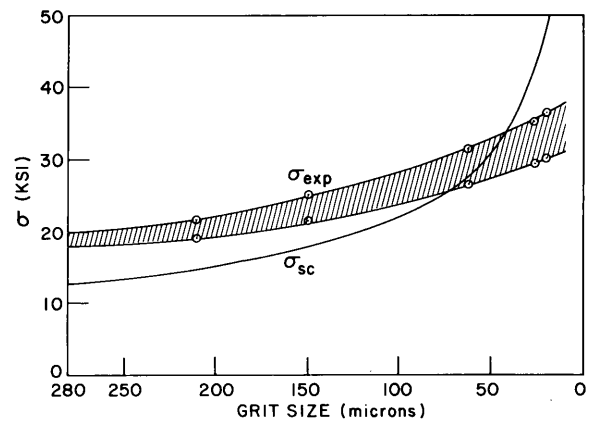

Fig. 7 - Fracture stress of AlSiMag 614 vs size of SiC finishing grit, both calculated from surface crack fracture theory (σ_{SC}) and determined experimentally (σ_{EXP}). The upper bound of σ_{EXP} represents the numerical average, and the lower bound shows two average standard deviations below the mean.

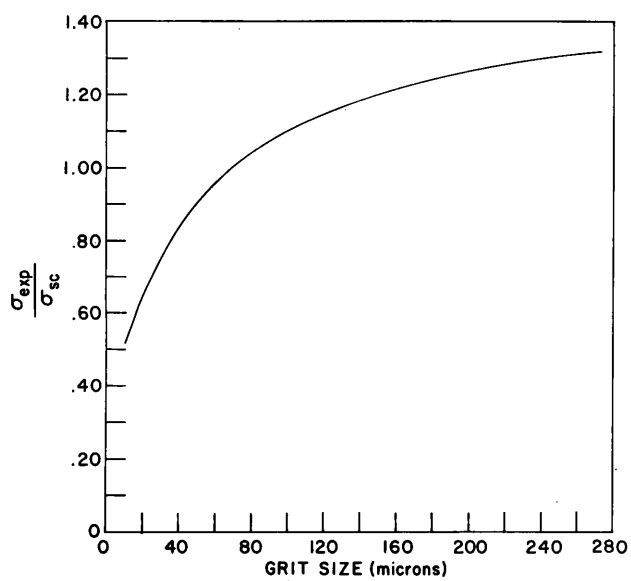

Fig. 8 - Ratio of two standard deviations below the mean fracture stress to the fracture stress computed using surface crack fracture theory vs size of SiC finishing grit for AlSiMag 614

REFERENCES

1. Bersch, C.F., "Properties of Ceramics for Structural and/or High Temperature Use: Need for Control, Measurement and Compilation," Symposium on Mechanical and Thermal Properties of Ceramics, 1-2 April 1968, Proceedings of the Symposium not yet published

2. Tiffany, C.F., and Lorenz, P.M., "An Investigation of Low Cycle Fatigue Failures Using Applied Fracture Mechanics," Boeing Company, Tech. Documentary Report ML-TDR-64-53, Contract AF 33(657)-10251, May 1964

3. Baxter, W.T., "Jewelry, Gem Cutting, and Metalcraft," Third Edition, New York: Whittlesey House, pp. 178-181, 1950

4. The Carborundum Company, private communication

5. "Navy Uses Fracture Tester to Select Materials for Ocean Research," Test Engineering and Management. XXI (No. 2):26, 27, 30 (Feb. 1969)

6. Irwin, G.R., "Crack-Extension Force for a Part-Through Crack in a Plate," J. Appl. Mech. 29(No. 4):651-654 (Dec. 1962)

7. McKinney, K.R., "Fracture Toughness of Ceramic Materials Using the Single-Edge-Notched Specimen," NRL Memorandum Report 1931, p. 6, Sept. 1968

8. Roark, R.J., "Formulas for Stress and Strain," New York:McGraw-Hill, p. 194, 1954

9. Report on Coors-NRL Joint Project (not published yet)

Appendix A
DETERMINATION OF BEARING RADIUS

The use of the equation

$$\sigma = \frac{3W}{2\pi mt^2}\left[m + (m + 1)\log\frac{\alpha}{r_o} - (m - 1)\frac{r_o^2}{4\alpha^2}\right] \tag{A1}$$

illustrated by Roark (8) poses some problems. Observe that if one uses r_o equal to 0, then assumes that a point force is applied to the specimen, σ becomes infinite. What then should be done with r_o? No method of direct measurement comes to mind; however an indirect one does. If by the use of strain gages one obtains the information necessary to calculate the stress immediately opposite the bearing point for any particular load, it would then be possible to compute effective r_o for any stress up to the fracture stress. Several interesting observations are: one, depending on the properties of the specimen used, r_o is a function of the stress; two, since a strain gage cannot sample a point, several sizes of strain gages must be used so that extrapolation to zero strain gage size can be done; three, ideally the procedure must be done for every material and for every difference in size; practically, it may not be necessary; and four, for similar specimens, any bending or edge effects would be incorporated into effective r_o.

Consider the case of the two materials, soda lime glass and AD-99 alumina. Nine specimens of each were prepared in three groups, each group having a different size strain gage centrally located on one surface. Data were then recorded for each specimen and can be seen in Tables A1 through A18. The averages for each size strain gage can be seen in Tables A19 through A24. These tables are illustrated graphically along with the extrapolation to zero strain gage length in Figs. A1 and A2. From these figures, and the use of the equation from Roark, one can compute the data shown in Fig. A3. This shows that

$$\text{eff. } r_o = f(\sigma). \tag{A2}$$

Roark's equation could then be changed to

$$\sigma_{EXP} = \frac{3W}{2\pi mt^2}\left[m + (m + 1)\log\left(\frac{\alpha}{f(\sigma_{EXP})}\right) - (m - 1)\frac{f(\sigma_{EXP})^2}{4\alpha^2}\right]. \tag{A3}$$

It is evident that $f(\sigma_{EXP})$ differs from one material and/or specimen configuration to another. While the causes of these differences are certainly important as well as interesting, they are not critical to the subject at hand, and therefore will not be further investigated here.

Applying Eq. (A2) and (A3) to the information about the specific examples used here we find that for soda-lime glass

$$\text{eff. } r_o = 0.110, \tag{A4}$$

$$\sigma_{EXP} = \frac{3 \times 10^{-3}W}{2\pi mt^2}\left[m + (m + 1)\log\left(\frac{\alpha}{0.110}\right) - (m - 1)\left(\frac{0.110}{2\alpha}\right)^2\right] \tag{A5}$$

and for AD-99 alumina

$$\text{eff. } r_o = -0.00158\sigma + 0.133 \tag{A6}$$

$$\sigma_{EXP} = \frac{3 \times 10^{-3} W}{2\pi mt^2} \left[m + (m+1) \log \left(\frac{a}{-0.00158\,\sigma_{EXP} + 0.133} \right) - (m-1) \left(\frac{-0.00158\sigma_{EXP} + 0.133}{2a} \right)^2 \right], \quad (A7)$$

where eff. r_o is effective bearing radius in inches, σ_{EXP} the stress in ksi, W the load in pounds, m the reciprocal of Poisson's ratio, t the specimen thickness in inches, and α the radius of the part of the specimen being tested, in inches.

The range of validity for Eqs. (A4) through (A7) is from σ_{EXP} = 1 ksi to fracture stress. However, they should be used with caution for $\sigma_{EXP} > 40$ ksi, since no data were available for these high stresses.

The above procedure can be carried out any time it seems necessary. Exactly what this means is not now known; however, observe that, if the soda-lime-glass equation were used for AD-99 alumina, or vice versa, a less than 10% error would result for the stresses that normally cause their fracture in dynamic testing. This seems ironic, since about the only things that these two materials have in common is that they are both nonmetallic and were, in general terms, subjected to the same test.

Table A1
Soda-Lime Glass Specimen
No. 1 with .125 in. Gage
$E = 10 \times 10^6$ lb/in.^{2}

Load (lb)	Microstrain $\left(\frac{\text{in.}}{\text{in.}} \times 10^{-6}\right)$	Stress $\left(\frac{\text{lb}}{\text{in.}^2}\right)$
4	260	2600
8	517	5170
12	769	7690
16	1029	10290
20	1301	13010
24	1563	15630
28	1796	17960

Table A2
Soda-Lime Glass Specimen
No. 2 with .125 in. Gage
$E = 10 \times 10^6$ lb/in.^{2}

Load (lb)	Microstrain $\left(\frac{\text{in.}}{\text{in.}} \times 10^{-6}\right)$	Stress $\left(\frac{\text{lb}}{\text{in.}^2}\right)$
4	240	2400
8	478	4780
12	710	7100
16	968	9680
20	1236	12360
24	1513	15130
28	1715	17150
32	1974	19740

Table A3
Soda-Lime Glass Specimen
No. 3 with .125 in. Gage
$E = 10 \times 10^6$ lb/in.^{2}

Load (lb)	Microstrain $\left(\frac{\text{in.}}{\text{in.}} \times 10^{-6}\right)$	Stress $\left(\frac{\text{lb}}{\text{in.}^2}\right)$
4	235	2350
8	482	4820
12	756	7560
16	1006	10060
20	1248	12480
24	1512	15120
28	1764	17640

Table A4
Soda-Lime Glass Specimen
No. 1 with .063 in. Gage
$E = 10 \times 10^6$ lb/in.^{2}

Load (lb)	Microstrain $\left(\frac{\text{in.}}{\text{in.}} \times 10^{-6}\right)$	Stress $\left(\frac{\text{lb}}{\text{in.}^2}\right)$
4	287	2870
8	550	5500
12	844	8440
16	1115	11150
20	1403	14030

Table A5
Soda-Lime Glass Specimen
No. 2 with .063 in. Gage
$E = 10 \times 10^6$ lb/in.^{2}

Load (lb)	Microstrain $\left(\frac{\text{in.}}{\text{in.}} \times 10^{-6}\right)$	Stress $\left(\frac{\text{lb}}{\text{in.}^2}\right)$
4	279	2790
8	595	5950
12	884	8840
16	1194	11940
20	1474	14740
24	1784	17840
28	2089	20890

Table A6
Soda-Lime Glass Specimen
No. 3 with .063 in. Gage
$E = 10 \times 10^6$ lb/in.^{2}

Load (lb)	Microstrain $\left(\frac{\text{in.}}{\text{in.}} \times 10^{-6}\right)$	Stress $\left(\frac{\text{lb}}{\text{in.}^2}\right)$
4	221	2210
8	548	5480
12	850	8500
16	1122	11220
20	1415	14150
24	1690	16900

Table A7
Soda-Lime Glass Specimen
No. 1 with .032 in. Gage
$E = 10 \times 10^6$ lb/in.^{2}

Load (lb)	Microstrain $\left(\frac{\text{in.}}{\text{in.}} \times 10^{-6}\right)$	Stress $\left(\frac{\text{lb}}{\text{in.}^2}\right)$
4	238	2380
8	487	4870
12	708	7080
16	943	9430
20	1173	11730
24	1418	14180
28	1598	15980

Table A8
Soda-Lime Glass Specimen
No. 2 with .032 in. Gage
$E = 10 \times 10^6$ lb/in.^{2}

Load (lb)	Microstrain $\left(\frac{\text{in.}}{\text{in.}} \times 10^{-6}\right)$	Stress $\left(\frac{\text{lb}}{\text{in.}^2}\right)$
4	354	3540
8	649	6490
12	989	9890
16	1324	13240
20	1669	16690
24	1984	19840

Table A9
Soda-Lime Glass Specimen
No. 3 with .032 in. Gage
$E = 10 \times 10^6$ lb/in.^{2}

Load (lb)	Microstrain $\left(\frac{\text{in.}}{\text{in.}} \times 10^{-6}\right)$	Stress $\left(\frac{\text{lb}}{\text{in.}^2}\right)$
4	294	2940
8	649	6490
12	985	9850
16	1295	12950
20	1659	16590

Table A10
AD-99 Alumina Specimen
No. 1 with .125 in. Gage
$E = 50 \times 10^6$ lb/in.^{2}

Load (lb)	Microstrain $\left(\frac{\text{in.}}{\text{in.}} \times 10^{-6}\right)$	Stress $\left(\frac{\text{lb}}{\text{in.}^2}\right)$
5	5	250
10	17	850
15	35	1750
20	52	2600
25	67	3350
30	83	4150
35	104	5200
40	119	5950
45	136	6800
50	154	7700
55	171	8550
60	189	9450
65	207	10350
70	221	11050
75	241	12050
80	259	12950
85	276	13800
90	294	14700
95	314	15700
100	330	16500
105	350	17500

Table A11
AD-99 Alumina Specimen
No. 2 with .125 in. Gage
$E = 50 \times 10^6$ lb/in.^{2}

Load (lb)	Microstrain $\left(\frac{\text{in.}}{\text{in.}} \times 10^{-6}\right)$	Stress $\left(\frac{\text{lb}}{\text{in.}^2}\right)$
5	17	850
10	36	1800
15	50	2500
20	68	3400
25	84	4200
30	100	5000
35	119	5950
40	135	6750
45	154	7700
50	170	8500
55	189	9450
60	206	10300
65	223	11150
70	240	12000
75	259	12950
80	276	13800
85	292	14600
90	311	15550
95	327	16350
100	346	17300
105	364	18200
110	380	19000

Table A12
AD-99 Alumina Specimen
No. 3 with .125 in. Gage
$E = 50 \times 10^6$ lb/in.^{2}

Load (lb)	Microstrain $\left(\frac{\text{in.}}{\text{in.}} \times 10^{-6}\right)$	Stress $\left(\frac{\text{lb}}{\text{in.}^2}\right)$
5	18	900
10	33	1650
15	50	2500
20	70	3500
25	88	4400
30	100	5000
35	122	6100
40	138	6900
45	155	7750
50	173	8650
55	192	9600
60	210	10500
65	228	11400
70	243	12150
75	259	12950
80	279	13950
85	298	14900
90	314	15700
95	333	16650
100	354	17700
105	368	18400

Table A13
AD-99 Alumina Specimen
No. 1 with .063 in. Gage
$E = 50 \times 10^6$ lb/in.^{2}

Load (lb)	Microstrain $\left(\frac{\text{in.}}{\text{in.}} \times 10^{-6}\right)$	Stress $\left(\frac{\text{lb}}{\text{in.}^2}\right)$
5	11	550
10	27	1350
15	45	2250
20	65	3250
25	84	4200
30	98	4900
35	119	5950
40	138	6900
45	158	7900
50	175	8750
55	194	9700
60	214	10700
65	234	11700
70	251	12550
75	270	13500

Table A14
AD-99 Alumina Specimen
No. 2 with .063 in. Gage
$E = 50 \times 10^6$ lb/in.^{2}

Load (lb)	Microstrain $\left(\frac{\text{in.}}{\text{in.}} \times 10^{-6}\right)$	Stress $\left(\frac{\text{lb}}{\text{in.}^2}\right)$
5	5	250
10	23	1150
15	43	2150
20	64	3200
25	86	4300
30	102	5100
35	125	6250
40	145	7250
45	163	8150
50	184	9200
55	205	10250
60	226	11300
65	247	12350
70	266	13300
75	288	14400
80	307	15350
85	327	16350
90	350	17500
95	370	18500
100	392	19600
105	411	20550
110	433	21650
115	460	23000

Table A15
AD-99 Alumina Specimen
No. 3 with .063 in. Gage
$E = 50 \times 10^6$ lb/in.^{2}

Load (lb)	Microstrain $\left(\frac{\text{in.}}{\text{in.}} \times 10^{-6}\right)$	Stress $\left(\frac{\text{lb}}{\text{in.}^2}\right)$
5	19	950
10	35	1750
15	50	2500
20	71	3550
25	88	4400
30	106	5300
35	126	6300
40	145	7250
45	165	8250
50	182	9100
55	201	10050
60	222	11100
65	244	12200
70	261	13050
75	282	14100
80	300	15000
85	322	16100
90	342	17100
95	361	18050
100	383	19150
105	403	20150
110	420	21000
115	444	22200

Table A16
AD-99 Alumina Specimen
No. 1 with .032 in. Gage
$E = 50 \times 10^6$ lb/in.^{2}

Load (lb)	Microstrain $\left(\frac{\text{in.}}{\text{in.}} \times 10^{-6}\right)$	Stress $\left(\frac{\text{lb}}{\text{in.}^2}\right)$
5	14	700
10	33	1650
15	55	2750
20	77	3850
25	97	4850
30	117	5850
35	137	6850
40	158	7900
45	182	9100
50	201	10050
55	222	11100
60	245	12250
65	264	13200
70	283	14150
75	306	15300
80	327	16350
85	348	17400
90	372	18600
95	395	19750
100	414	20700
105	435	21750
110	458	22900

Table A17
AD-99 Alumina Specimen
No. 2 with .032 in. Gage
$E = 50 \times 10^6$ lb/in.^{2}

Load (lb)	Microstrain $\left(\frac{\text{in.}}{\text{in.}} \times 10^{-6}\right)$	Stress $\left(\frac{\text{lb}}{\text{in.}^2}\right)$
5	17	850
10	35	1750
15	54	2700
20	76	3800
25	94	4700
30	114	5700
35	133	6650
40	152	7600
45	172	8600
50	192	9600
55	214	10700
60	236	11800
65	257	12850
70	274	13700
75	298	14900
80	318	15900
85	339	16950
90	360	18000
95	382	19100
100	402	20100
105	424	21200
110	443	22150

Table A18
AD-99 Alumina Specimen
No. 3 with .032 in. Gage
$E = 50 \times 10^6$ lb/in.^{2}

Load (lb)	Microstrain $\left(\frac{\text{in.}}{\text{in.}} \times 10^{-6}\right)$	Stress $\left(\frac{\text{lb}}{\text{in.}^2}\right)$
5	14	700
10	30	1500
15	49	2450
20	66	3300
25	85	4250
30	101	5050
35	125	6250
40	141	7050
45	162	8100
50	181	9050
55	203	10150
60	221	11050
65	243	12150
70	263	13150
75	282	14100
80	306	15300
85	326	16300
90	347	17350
95	370	18500
100	390	19500
105	412	20600
110	431	21550
115	455	22750
120	475	23750
125	496	24800

Table A19
Soda-Lime Glass Average Stresses Using .125 in. Gage

Load (lb)	Stress $\left(\frac{lb}{in.^2}\right)$
4	2450
8	4923
12	7450
16	10010
20	12617
24	15293
28	17583
32	19740*

Table A20
Soda-Lime Glass Average Stresses Using .063 in. Gage

Load (lb)	Stress $\left(\frac{lb}{in.^2}\right)$
4	2623
8	5643
12	8593
16	11437
20	14307
24	17370*
28	20890*

Table A21
Soda-Lime Glass Average Stresses Using .032 in. Gage

Load (lb)	Stress $\left(\frac{lb}{in.^2}\right)$
4	2953
8	5950
12	8940
16	11873
20	15003
24	17010*
28	15980*

*Three values not available for this average.

Table A22
AD-99 Alumina Average Stresses Using .125 in. Gage

Load (lb)	Stress $\left(\frac{lb}{in.^2}\right)$
5	667
10	1433
15	2250
20	3167
25	3983
30	4717
35	5750
40	6533
45	7417
50	8283
55	9200
60	10083
65	10967
70	11733
75	12650
80	13567
85	14433
90	15317
95	16233
100	17167
105	18033
110	19000*

Table A23
AD-99 Alumina Average Stresses Using .063 in. Gage

Load (lb)	Stress $\left(\frac{lb}{in.^2}\right)$
5	583
10	1417
15	2300
20	3333
25	4300
30	5100
35	6167
40	7133
45	8100
50	9017
55	10000
60	11033
65	12083
70	12967
75	14000
80	15175*
85	16225*
90	17300*
95	18275*
100	19375*
105	20350*
110	21325*
115	22600*

Table A24
AD-99 Alumina Average Stresses Using .032 in. Gage

Load (lb)	Stress $\left(\frac{lb}{in.^2}\right)$
5	750
10	1633
15	2633
20	3650
25	4600
30	5533
35	6583
40	7517
45	8600
50	9567
55	10650
60	11700
65	12733
70	13667
75	14767
80	15850
85	16833
90	17983
95	19117
100	20100
105	21183
110	22200
115	22750*
120	23750*
125	24800*

*Three values not available for this average.

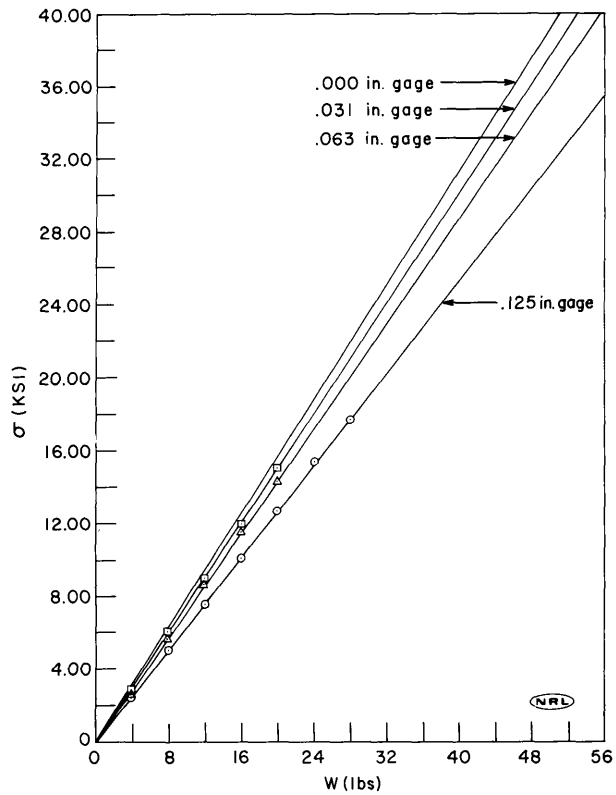

Fig. A1 - Experimental stress (σ) indicated using a strain gage directly opposite a 1-in.-diameter loading nose vs load (W) for soda-lime glass 0.049 in. thick mounted on a 2.375-in.-diameter ring. Shown are curves for three different gages with extrapolation to zero strain gage length.

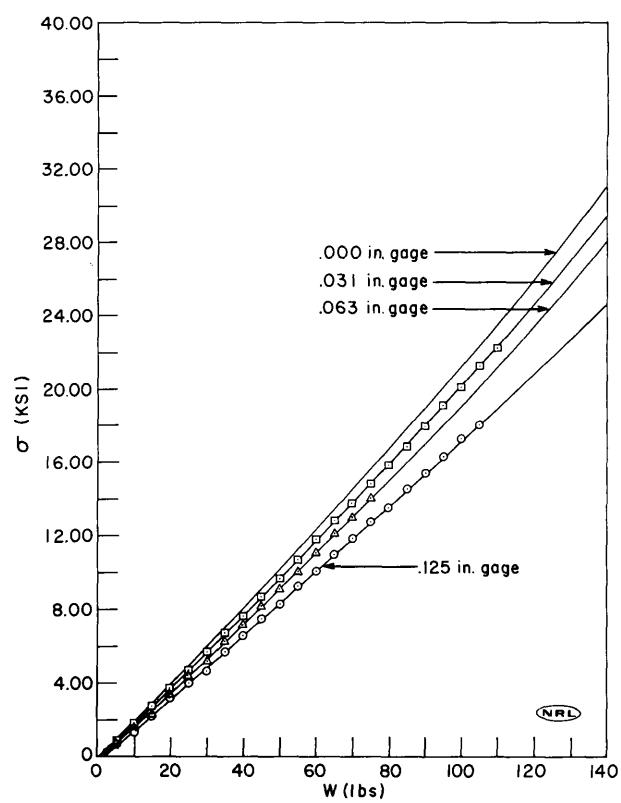

Fig. A2 - Experimental stress (σ) indicated using a strain gage directly opposite a 1-in.-diameter loading nose vs load (W) for AD-99 alumina 0.100 in. thick mounted on a 3.375-in.-diameter ring. Shown are curves for three different length gages with extrapolation to zero strain gage length.

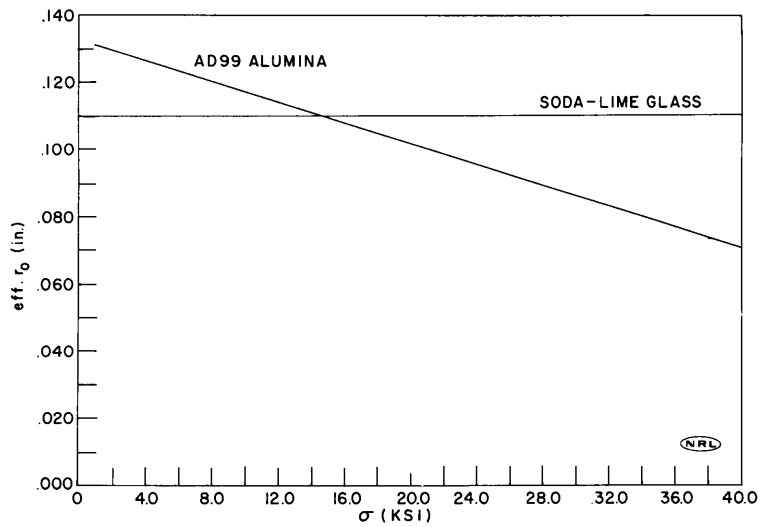

Fig. A3 - Effective bearing radius (eff. r_o) vs stress (σ) directly opposite loading nose for 0.100-in.-thick AD-99 alumina mounted on a 3.375-in.-diameter ring and 0.049-in.-thick soda-lime glass mounted on a 2.375-in.-diameter ring

Appendix B
SURFACE ANALYSIS

It has been stated that the flaw size produced, s, relative to the size of grit used in a final polish, d, decreases as the grit becomes larger, or $d^2s/dd^2 \leq 0$ for all values of d that have both physical and practical significance. Profilometer results serve to support this assumption, provided it holds that a similar grinding procedure with various size grits produces a similar pattern on the surface of the material. This being the case, the ratio of profilometer readings, AA-arithmetic average, is indicative of the ratio of surface flaw damage from one specimen to another. The similar-patterns assumption is necessary because it is possible for very different surface patterns to result in similar profilometer results.* The results of the profilometer determination for each surface finish along with the effective grit size is seen in Table B1 (3,4). Effective grit size is here defined as: the size of sufficiently hard grit used with sufficient grinding pressure to cause the damage observed, thus validating the original assumption in the main text regarding grit size and damage caused. The computation of effective grit size was based on the No. 400 grit rather than No. 600 grit, because information on No. 400 grit was more readily available and probably more reliable. Applying the effective grit size in place of the actual grit size in Fig. 7, it is observed that the value for average σ_{EXP} for No. 220 grit lies closer to the σ_{SC} curve, and the two points on the σ_{EXP} curve, 97% of all surface, that are on the large grit size side of the crossover point now lie much nearer to the σ_{SC} curve.

Further investigations of the surfaces, done using a microscope, are seen in Figs. B1 through B6. On close inspection of these figures one can observe the directionality of the grinding in the "as paralleled" case - also the change in roughness from one grinding grit size to another while the pattern remains essentially the same.

Table B1
Comparison of Surface Finishes Obtained on AlSiMag 614
Using Various SiC Abrasive Powders

Grit No.	Actual Grit Size (microns)	Profilometer[o] Reading (AA microinches)	Profilometer* Reading Ratio	Effective Grit Size (microns)	Profilometer[x] Reading (AA microinches)	Profilometer[x]* Reading Ratio	Effective Grit Size (microns)
600	17 (4)	16	.80	21	18	.75	20
400	26 (3)	20	1.00	26	24	1.00	26
220	62 (3)	40	2.00	52	40	1.67	43
100	149 (3)	100	5.00	130	100	4.17	108
70	210 (3)	125	6.25	163	140	5.84	152

[o]Median value.
*Compared to Grit No. 400.
[x]Highest values (worst flaw area).

*Technical Bulletin on Surface Texture, Micrometrical Manufacturing Co., pp. 4-5.

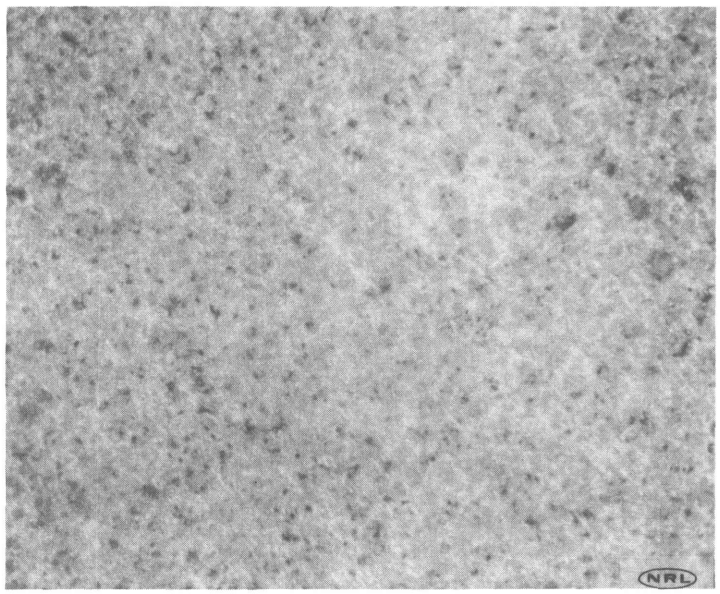

Fig. B1 - The surface (X145) of an AlSiMag 614 specimen after being flattened and paralleled on a Gallmeyer and Livingston surface grinder using a 100-grit and 100-concentration resinoid-bond diamond grinding wheel

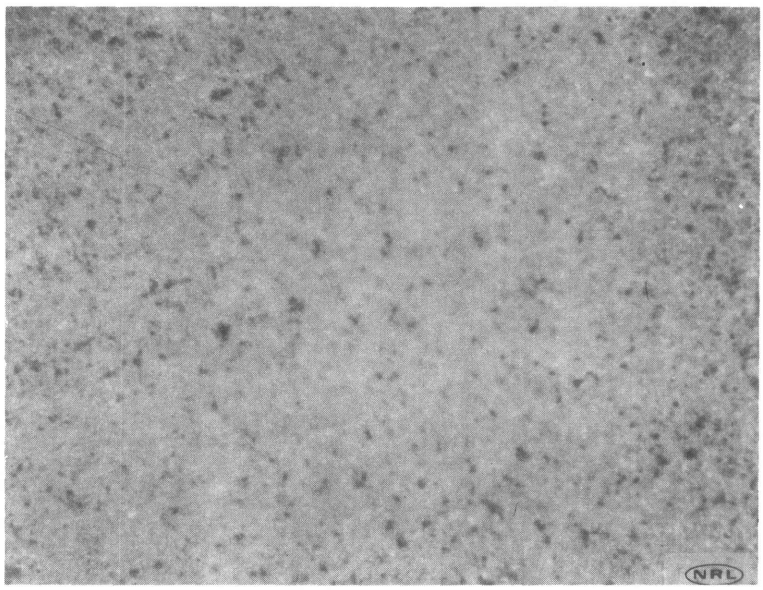

Fig. B2 - The surface (X145) of an AlSiMag 614 specimen flattened, paralleled, and finished on a Strasbaugh optical grinding machine with No. 600 SiC grit

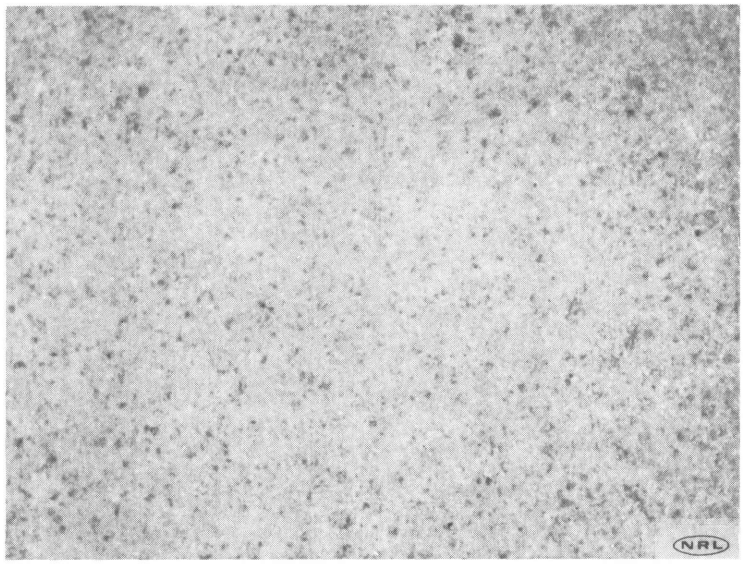

Fig. B3 - The surface (X145) of an AlSiMag 614 specimen flattened, paralleled, and finished on a Strasbaugh optical grinding machine with No. 400 SiC grit

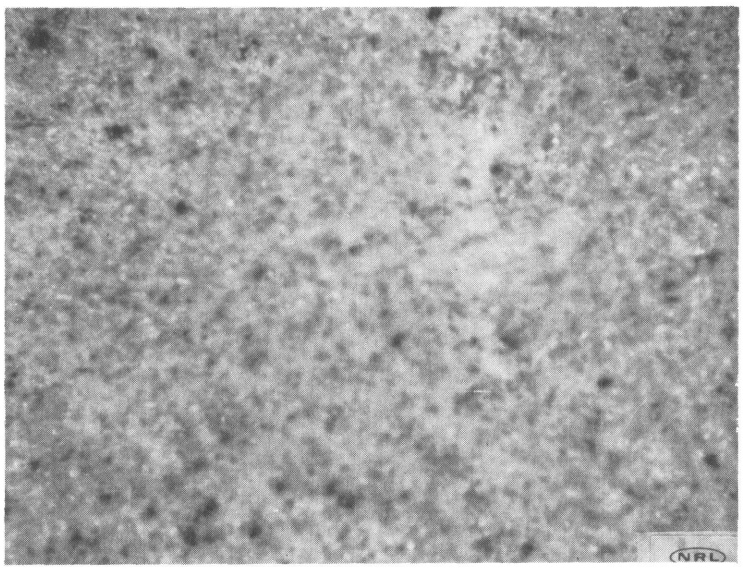

Fig. B4 - The surface (X145) of an AlSiMag 614 specimen flattened, paralleled, and finished on a Strasbaugh optical grinding machine with No. 200 SiC grit

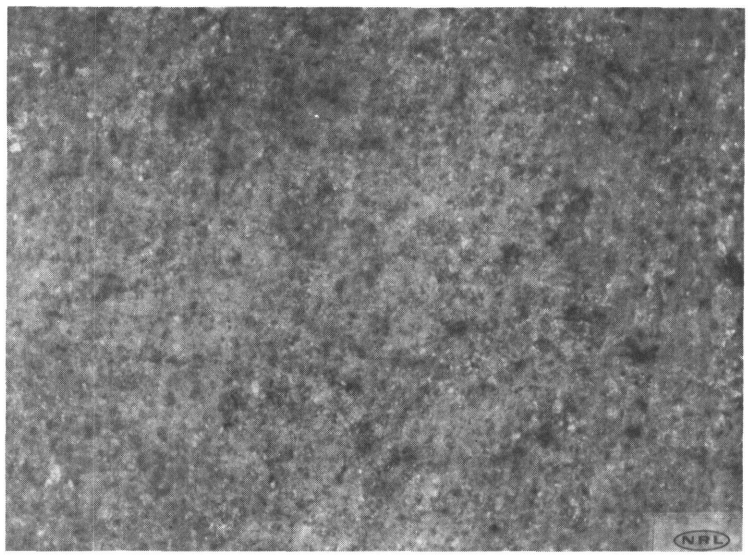

Fig. B5 - The surface (X145) of an AlSiMag 614 specimen flattened, paralleled, and finished on a Strasbaugh optical grinding machine with No. 100 SiC grit

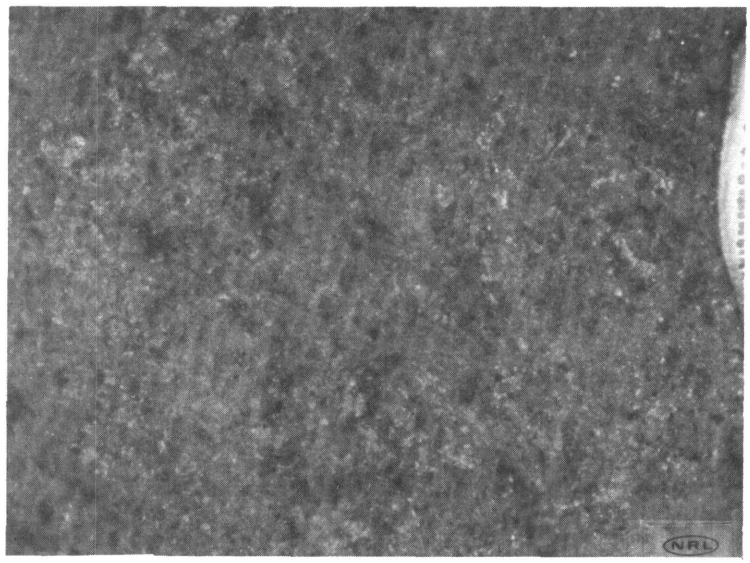

Fig. B6 - The surface (X145) of an AlSiMag 614 specimen flattened, paralleled, and finished on a Strasbaugh optical grinding machine with No. 70 SiC grit

This page intentionally left blank.

Security Classification

DOCUMENT CONTROL DATA - R & D

(Security classification of title, body of abstract and indexing annotation must be entered when the overall report is classified)

1. ORIGINATING ACTIVITY *(Corporate author)* Naval Research Laboratory Washington, D.C. 20390	2a. REPORT SECURITY CLASSIFICATION Unclassified 2b. GROUP

3. REPORT TITLE

THE EFFECT OF SURFACE FINISHING ON STRUCTURAL-CERAMIC FAILURE

4. DESCRIPTIVE NOTES *(Type of report and inclusive dates)*

Interim report on one phase of the problem; work is continuing.

5. AUTHOR(S) *(First name, middle initial, last name)*

Karl R. McKinney and Charles M. Herbert

6. REPORT DATE November 5, 1969	7a. TOTAL NO. OF PAGES 28	7b. NO. OF REFS 9
8a. CONTRACT OR GRANT NO. NRL Problem 84F01-05 b. PROJECT NO. A-32-520/652/69 R0070201 c. d.	9a. ORIGINATOR'S REPORT NUMBER(S) NRL Report 6942 9b. OTHER REPORT NO(S) *(Any other numbers that may be assigned this report)*	

10. DISTRIBUTION STATEMENT

This document has been approved for public release and sale; its distribution is unlimited.

11. SUPPLEMENTARY NOTES	12. SPONSORING MILITARY ACTIVITY Department of the Navy (Naval Air Systems Command), Washington, D.C. 20360

13. ABSTRACT

A relationship between fracture strength and surface finish of brittle non-metallic materials was examined and related to surface crack theory. An experimental illustration used AlSiMag 614, a 94% pure alumina with a near zero porosity. Specimen disks 3.625 + 0.031 in. in diameter by 0.085 + 0.010 in. thick were prepared, each having a specific surface finish. Testing was done with a biaxial ball and ring test. Observations were made regarding other materials and other abrasive powders.

DD FORM 1 NOV 65 1473 (PAGE 1)

S/N 0101-807-6801

Security Classification

Security Classification

14. KEY WORDS	LINK A ROLE	LINK A WT	LINK B ROLE	LINK B WT	LINK C ROLE	LINK C WT
Ceramic finishing						
Surface crack theory						
Strength of ceramics						
Fracture						
Biaxial testing						

DD FORM 1 NOV 65 1473 (BACK)
(PAGE 2)

Security Classification